Journal of Ship Research, Vol. 67, No. 4, December 2023, pp. 235–251
http://dx.doi.org/10.5957/JOSR.02230004

Journal of
Ship Research

Unmanned Underwater Vehicle Autonomy and Control near Submarines Using Actively Sampled Surrogates

Brady M. Hammond[*,†] and **Themistoklis P. Sapsis**[†]

[*]*Naval Construction and Engineering, United States Navy, Massachusetts Institute of Technology, 77 Massachusetts Avenue, Cambridge*
[†]*Department of Mechanical Engineering, Massachusetts Institute of Technology, 77 Massachusetts Avenue, Cambridge, MA*

Many tools have been developed to simulate unmanned underwater vehicle (UUV) motion and autonomous behaviors to evaluate UUV capabilities. However, there is no simulator that performs real-time modeling of the complex hydrodynamic interaction forces that a UUV experiences when operating near a moving submarine. These hydrodynamic interactions must be determined in real time to simulate the launch and recovery of UUVs from submarines. Potential flow models may be fast enough to solve the hydrodynamic interactions in real time, but by oversimplifying the physics and neglecting viscosity, they introduce inaccuracies into the simulations. Computational fluid dynamics (CFD) is capable of accurately modeling these hydrodynamic interactions, but simulations take hours or days to solve. To overcome this obstacle, a machine learning method known as Gaussian process (GP) regression is used to create a surrogate reduced-order-model that predicts the hydrodynamic interactions in real time. The GP regression model is trained by actively sampling CFD simulations in order to accurately model complex hydrodynamic interactions. This new approach allows the GP regression model to be incorporated into a UUV motion simulator and evaluate how the UUV is affected by the hydrodynamic interactions. Operating envelopes are developed that outline regions where the UUV safely overcomes the hydrodynamic interactions and where the UUV is overpowered and collides with the submarine. By incorporating this surrogate model into the autonomy architecture, new autonomous behaviors are created that compensate for the hydrodynamic interactions by adjusting the desired UUV heading and speed which allows it to better stay on course.

Keywords: unmanned marine vehicle; maneuvering simulation; hydrodynamic interaction; Gaussian process regression; active sampling machine learning; reduced order modeling; launch and recovery

1. Introduction

Several efforts have been made to model the hydrodynamic interaction forces acting on an unmanned underwater vehicle (UUV) when it operates near a moving submarine (Fedor 2009; Leong 2014; Du et al. 2018). These unwanted hydrodynamic interactions push and rotate the UUV and may cause it to become uncontrollable or collide with the submarine (Leong 2014). Real-time modeling of these hydrodynamic interactions is essential to simulate the motion required to launch and recover UUVs from submarines because the UUV control surfaces and propeller respond to real-time changes in the state of the UUV (Prestero 2001; Fossen 2011). There is no existing method that enables the real-time accurate modeling of these complex hydrodynamic interaction forces that a UUV experiences when operating near a moving submarine. Recently, a surrogate reduced-order model (ROM) of the hydrodynamic interactions between a UUV and submarine was developed that is capable of predicting these

Manuscript received at SNAME headquarters February 27, 2023; revised manuscript received October 22, 2023; published online November 29, 2023.
Corresponding author: Themistoklis P. Sapsis, sapsis@mit.edu

forces and moments in real time (Hammond & Sapsis 2023). This study explores incorporating this surrogate model into a UUV motion simulator in order to explore how the hydrodynamic interactions impact the ability of the UUV to maneuver around the submarine.

Potential flow is a series of hydrodynamic equations and assumptions that model a fluid as irrotational, inviscid, and incompressible (Fossen 2011; Newman 2017). Potential flow models are often simple enough to be solved in real time, but the oversimplified underlying physics result in inaccuracies when predicting the hydrodynamic interactions between two vehicles. These assumptions also result in the d'Alembert paradox, which predicts no hydrodynamic forces acting on a nonlifting body moving with constant translational velocity (Newman 2017). This is especially problematic when the UUV heading is not parallel to the flow (Jayarathne et al. 2014). Computational fluid dynamics (CFD) does not make these oversimplified assumptions and has been validated to accurately predict real-world hydrodynamic interactions between submarines and UUVs (Fedor 2009; Leong 2014). However, CFD often takes hours or days to determine the hydrodynamic interaction forces and moments for one single simulation of a UUV at a specific position, heading, and speed. For this reason, the hydrodynamic interactions modeled with the accuracy of CFD have not been able to be integrated into a UUV simulator.

In a recent study, a nonmyopic active sampling approach combined with Gaussian process (GP) regression is used to efficiently develop a ROM capable of predicting the UUV and submarine hydrodynamic interactions (Hammond & Sapsis 2023). This surrogate model is able to predict, with minimal computational cost, the hydrodynamic interaction forces and moments in real-time based on the UUV size, position, speed, and heading. The resulting GP surrogate model is trained using a minimal set of CFD simulations of a UUV operating near a submarine. The developed approach enables the surrogate model to predict these complex hydrodynamic interactions based on the accurate physics of the CFD simulations but without the typical computational expense of CFD modeling. To this end, this surrogate bridges the gap between accurate physics and real-time computational capacity, paving the way for real-time control methods.

Integrating this surrogate model into UUV motion simulators enables a better understanding of the current UUV autonomy and control capabilities. This is accomplished by using the forces and moments of the surrogate model in the equations of motion in order to determine how they impact the UUV. As the UUV position, speed, and heading change, the surrogate is capable of predicting the hydrodynamic interactions in real-time to see how the autonomous system responds to these forces and moments. This allows for the rapid exploration of which UUV maneuvers can be successfully performed around a submarine. Additionally, this allows for the rapid testing of new autonomous behaviors designed to overcome unwanted hydrodynamic interactions and improve launch and recovery maneuvering.

This paper begins by describing the method to incorporate the active sampled GP regression model into the UUV motion simulator. This starts with an overview of the UUV autonomy architecture and how each component is used to simulate UUV motion. Next, we provide a detailed description of how the GP regression is performed, as well as how the results are incorporated into the equations of motion and UUV autonomy architecture. We then discuss new autonomous behaviors for the UUV which use the surrogate model to impact the desired heading of the vehicle to better overcome the hydrodynamic interaction. Lastly, we discuss the results of the UUV simulations which incorporate the surrogate model into the UUV simulator. This includes the development of safe operating envelopes for the UUV under various conditions as it maneuvers around the submarine.

2. Methods

2.1. Approach

To simulate the motion of the UUV, a body-fixed coordinate system is located at the center of buoyancy of the UUV. The surge, sway, heave, roll, pitch, and yaw velocities and forces/moments are defined as u, v, w, p, q, r and X, Y, Z, K, M, N, respectively. The position of the UUV is expressed in the inertial reference frame using x, y, and z. Likewise, the roll, pitch, and yaw angles are denoted as ϕ, θ, and ψ. The forces and moments can also be nondimensionalized by the fluid density ρ, UUV speed u, and UUV length L_{UUV}, e.g., $X' = X/(0.5\rho u^2 L_{\text{UUV}}^2)$ or $N' = N/(0.5\rho u^2 L_{\text{UUV}}^3)$. The distances between the center of buoyancy and the center of gravity of the UUV in the three principle directions are defined as x_g, y_g, and z_g. This coordinate system is illustrated in Fig. 1.

Because experimentally attempting to study the hydrodynamic interactions between a submarine and UUV is both costly and has the risk of collision between the vehicles, a simulator is used to model the behavior and motion of a UUV. This simulator is designed using the framework outlined in the open-source UUV autonomy simulator known as MOOS-IvP (Benjamin et al. 2021). This framework uses three different vectors to relay information between apps within the simulator. These three different vectors are the state vector $\mathbf{x}$, input vector $\mathbf{u}$, and desired state vector $\mathbf{x_d}$ and are listed in equation (1). The propeller thrust and torque are denoted as X_{Prop} and K_{Prop}, respectively, while the rudder and stern plane angles are denoted as δ_r and δ_s, respectively.

$$\begin{aligned} \mathbf{x} &= [u, v, w, p, q, r, x, y, z, \phi, \theta, \psi]^T \\ \mathbf{u} &= [X_{\text{Prop}}, K_{\text{Prop}}, \delta_r, \delta_s]^T \\ \mathbf{x_d} &= [u_d, z_d, \psi_d]^T \end{aligned} \tag{1}$$

The MOOS-IvP architecture uses three basic apps to model the UUV control system and its impact on UUV motion. The pHelmIvP app takes in the state vector of the vehicle position and motion and uses an autonomous behavior to compute a desired state vector containing the new desired speed and heading. This

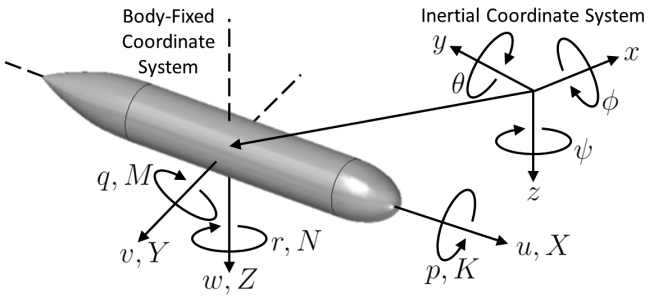

Fig. 1 Orientation of UUV body-fixed and inertial coordinate systems with their corresponding velocities, forces, and moments

desired state vector is passed to the pMarinePID app which simulates a proportional integral derivative (PID) controller to determine the input vector of the propeller thrust and torque, as well as the angle of the stern planes and rudder. This input vector, as well as the state vector, is then passed to the uSimMarine app which solves the equations of motion to determine the new state vector of the UUV, and the process is iterated. Figure 2 shows an overview of the simulation architecture.

While UUV simulators have been used extensively to model UUV missions, there are no known simulators that are able to model the hydrodynamic interactions between a UUV and a moving submarine with the accuracy of CFD (Leong 2014). This is because the forces and moments felt by the UUV need to be determined in real time in order to determine how the UUV and submarine hydrodynamic interactions impact the UUV motion. Real-time determinations of these hydrodynamic interactions are beyond current CFD capability. However, a GP regression machine learning surrogate model trained on CFD simulations can be used to predict the hydrodynamic interaction forces and moments on the UUV based on the state vector of the UUV (Hammond & Sapsis 2023). In this study, this new surrogate model is used to simulate how these hydrodynamic interactions impact the motion of a UUV as it maneuvers near a moving submarine.

2.2. Equations of motion away from boundaries

The total forces and moments exerted on the vehicle is the sum of the hydrostatic, damping, added mass, and control forces and moments. These forces and moments are expressed using hydrodynamic coefficients as specified in the standard SNAME notation (SNAME 1950). For example, N_{uv} represents a nonlinear hydrodynamic coefficient that when multiplied by the surge and sway velocities u and v returns the yaw moment that the vehicle experiences due to moving at those two velocities. There are a large number of terms that can be added together to determine each force and moment, but many of them are zero or negligible. Determining hydrodynamic coefficients can be performed using potential flow, slender body strip theory, CFD, or physical experiments on models (Prestero 2001; Fossen 2011; Newman 2017). Many simplifications are made to the overall equations of motion to reduce the effort needed to determine all of the hydrodynamic coefficients (Warner 1991; Prestero 2001; Fossen 2011).

- Three degrees of freedom – For simplicity, the full six degree of freedom equations are reduced to three by assuming that roll, pitch, and heave are zero. Because many UUVs have similar geometry in the xy and xz plane, the heave and pitch results are the same as the sway and yaw results (Prestero 2001). Roll is also assumed to have negligible impact on UUV motion due to vehicle symmetry (Warner 1991; Prestero 2001). This simplification drastically reduces the effort to model submarine and UUV hydrodynamic interactions while still capturing the fundamental behaviors and capabilities.
- Hydrostatics – UUVs are usually designed to be neutrally buoyant so the vehicle weight and buoyancy offset. Additionally, the center of gravity is located in approximately the same location in the xy plane as the center of buoyancy so all hydrostatic terms cancel out (Warner 1991; Prestero 2001).
- Body damping forces – The sway and yaw hydrodynamic coefficients for the coupled linear cross flow and angular velocity terms are found to be negligible (Prestero 2001). This includes Y_{vr} and N_{vr}. Also, assuming xy plane symmetry allows for the neglecting of drag-induced forces and moments like $Y_{u|u|}$ and $N_{u|u|}$.
- Added mass – By assuming xy and xz plane symmetry, the added mass tensor simplifies to zero except on the diagonal terms and for the $Y_{\dot{r}} = N_{\dot{v}}$ and $Z_{\dot{q}} = M_{53}$ terms.

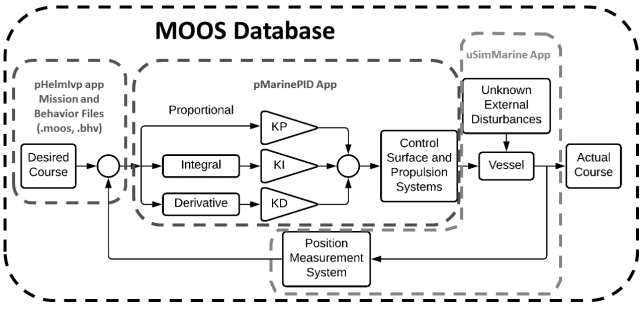

Fig. 2 Overlay of standard UUV control system block diagram with the MOOS-IvP architecture. This outlines the role of each app to fulfill its purpose of the control system

Applying these assumptions to the state, input, and desired input vectors results in the simplified vectors found in equation (2).

$$\begin{aligned} \mathbf{x} &= [u, v, r, x, y, \psi]^T \\ \mathbf{u} &= [X_{\text{Prop}}, \delta_r]^T \\ \mathbf{x_d} &= [u_d, \psi_d]^T \end{aligned} \tag{2}$$

These same assumptions are used to simplify the equations of motion of the UUV. These simplified equations of motion have been used in literature to simulate UUV maneuvering (Warner 1991; Prestero 2001; Fossen 2011). Some of these simulations have also been validated using real-world UUVs in sea trials (Warner 1991; Prestero 2001). These simplified equations of motion for the UUV are listed in equation (3).

$$\begin{bmatrix} m - X_{\dot{u}} & 0 & 0 \\ 0 & m - Y_{\dot{v}} & -Y_{\dot{r}} \\ 0 & -N_{\dot{v}} & I_{zz} - N_{\dot{r}} \end{bmatrix} \begin{bmatrix} \dot{u} \\ \dot{v} \\ \dot{r} \end{bmatrix} = \begin{bmatrix} X_{u|u|}u \mid u \mid +(X_{vr} + m)vr \\ +X_{rr}rr + X_{\text{Prop}} \\ Y_{v|v|}v \mid v \mid +Y_{r|r|}r \mid r \mid +Y_{uv}uv \\ +(Y_{ur} - m)ur + Y_{uu\delta_r}u^2\delta_r \\ N_{v|v|}v \mid v \mid +N_{r|r|}r \mid r \mid +N_{uv}uv \\ +N_{ur}ur + N_{uu\delta_r}u^2\delta_r \end{bmatrix} \tag{3}$$

The accelerations $\dot{u}$, $\dot{v}$, and $\dot{r}$ are computed by inverting the inertial matrix and multiplying it by the force vector. These accelerations are then numerically integrated using Euler's method along a small time interval Δt to determine the UUV linear and angular velocities, and then integrated again to find the UUV position and heading.

Equation (3) is ultimately used to determine the new state of the UUV based on the forces and moments acting on the vehicle. This is performed by the uSimMarine app which takes, as an

input, the previous state vector $\mathbf{x}$ and the input vector $\mathbf{u}$ of the propeller thrust X_{Prop} and rudder angle δ_r and returns the new position, speed, and heading of the UUV as a new state vector.

When a UUV operates in close proximity to a moving submarine, the submarine creates a wake and flow field around the submarine that affects the motion of the UUV. These equations of motion in equation (3) that use standard hydrodynamic coefficients do not account for these hydrodynamic interactions between a UUV and a submarine. To simulate the UUV motion near a submarine, the equations of motion need to be modified by replacing the UUV body forces and moments with the GP regression surrogate model forces and moments.

2.3. GP surrogate near the submarine

To simulate UUV motion near a moving submarine, the hydrodynamic interaction forces and moments acting on the UUV need to be determined each time it changes position, heading, or speed. This means that these hydrodynamic interactions need to be predicted in real time as the UUV maneuvers around the submarine. Because CFD usually takes hours or days to solve a simulation for one specific UUV in one particular position, heading, or speed, a ROM is used to predict these hydrodynamic interactions in real time. GP regression is used to create a surrogate ROM that predicts the surge, sway, and yaw hydrodynamic interaction forces and moments based on the state of the UUV. GP regression also provides estimates for the epistemic uncertainty or errors due to a lack of data. The GP regression model can be expressed as a random function,

$$y = f(x) + \epsilon \tag{4}$$

where $x \in \mathbb{R}^d$, $\epsilon \sim \mathcal{N}(0, \sigma^2)$ represents the noise of the model. The function f follows a Gaussian distribution with prescribed mean and covariance function (Rasmussen & Williams 2006):

$$f(x) \sim \mathcal{GP}(\mu(x), k(x, x')) \tag{5}$$

where $\mu(x)$ is the mean and $k(x, x')$ the covariance:

$$\mu(x) = \mathbb{E}[f(x)] \tag{6}$$

$$k(x, x') = \mathbb{E}[(f(x) - \mu(x))(f(x') - \mu(x'))] \tag{7}$$

GP regression can use one of many different covariance functions, which are also known as kernels. This study uses the popular radial basis function kernel with automatic relevance determination:

$$k(x, x') = \exp\left(\frac{-(x - x')^T \lambda^{-1} (x - x')}{2}\right) \tag{8}$$

where λ is the diagonal matrix containing the length scales of each input dimension. This kernel is selected because it mimics a Bayesian linear regression model with an infinite number of basic functions (Rasmussen & Williams 2006), which can take the form of any sufficiently smooth output function. Because the output function of the hydrodynamic interaction is unknown and complex, this kernel is opportune to map the output. Automatic relevance determination allows each input dimension to have a different length scale. This was necessary to implement in this GP regression model given the nature of the inputs of the UUV location, speed, size, and heading.

The objective of GP regression is to determine the predicted mean $y(\mathbf{X}_*)$ and covariance $K_{yy}(\mathbf{X}_*, \mathbf{X}'_*)$ for a given set of input-output data. The data set $\mathcal{D} = \{x_i, y_i\}_{i=1}^n$ is used to train the GP regression model where n is the number of samples in the data set. The input and output pairs are notated as $\mathbf{X} = [x_1, \ldots, x_n] \in \mathbb{R}^{d \times n}$ and $\mathbf{y} = [y_1, \ldots, y_n] \in \mathbb{R}^n$ where d is the dimension of the input domain. Likewise, $\mathbf{X}_* = [x_{*1}, \ldots, x_{*m}] \in \mathbb{R}^{d \times m}$ is a set of m locations for which a prediction is desired. The predicted mean and covariance at a set of points $\mathbf{X}_*$ are listed below as equations (9) and (10) (Rasmussen & Williams 2006):

$$y(\mathbf{X}_*) = K(\mathbf{X}_*, \mathbf{X})[K(\mathbf{X}, \mathbf{X}) + \sigma_n^2 \mathbf{I}]^{-1} \mathbf{y} \tag{9}$$

$$\begin{aligned} K_{yy}(\mathbf{X}_*, \mathbf{X}'_*) &= K(\mathbf{X}_*, \mathbf{X}'_*) \\ &- K(\mathbf{X}_*, \mathbf{X})[K(\mathbf{X}, \mathbf{X}) + \sigma_n^2 \mathbf{I}]^{-1} K(\mathbf{X}, \mathbf{X}'_*) \end{aligned} \tag{10}$$

The term σ_n^2 represents the aleatoric uncertainty in the training samples. This is a hyperparameter optimized by gradient descent methods to improve the performance of the GP regression (Rasmussen & Williams 2006). Additionally, it helps ensure the matrix in brackets in equations (9) and (10) is well-conditioned.

As the UUV changes position, heading, and speed, it experiences different forces and moments due to the hydrodynamic interactions between the vehicles. For this study, terms from the simplified state vector in equation (2) are used as inputs to the GP regression model. This allows the surrogate model to predict the hydrodynamic interactions based on changes to the UUV state vector. The x and y terms are nondimensionalized by the length of the submarine L_{Sub}. These nondimensional parameters are referred to as the Longitudinal Separation Ratio $R_{\text{long}} = x/L_{\text{Sub}}$ and Lateral Separation Ratio $R_{\text{lat}} = y/L_{\text{Sub}}$. In this study, the inertial coordinate system is fixed to the center of buoyancy of the submarine which is moving at a constant speed through the water. This fluid flow through the inertial frame caused by the submarine moving forward can be thought of as a current in a traditional earth-fixed inertial frame. Because of this flow, the sway velocity v and the heading angle ψ are not independent. This flow means that a nonzero heading angle in the inertial frame results in a nonzero sway velocity in the UUV body-fixed reference frame. This relationship is valid for small heading angles because the sway velocity is so much smaller than the UUV surge velocity or submarine velocity. As such, the GP surrogate only needed to account for the heading angle and not the redundant sway velocity to model the hydrodynamic interactions. Recognizing this dependence allows the input dimension of the surrogate model to be reduced which decreases the number of CFD simulations that need to be run in order to train the model. For the same reason, the yaw rate r is not used as an input to the surrogate model. Because a UUV is near parallel to the submarine during launch and recovery operations with no rapid heading changes, the yaw rate is very small compared to other terms and has negligible impact on hydrodynamic interactions. Not including this input in the surrogate allows the CFD simulations to be steady rather than unsteady. This drastically simplifies the CFD simulation complexity, decreases the simulation computational time, and reduces the number of simulations needed to explore the domain. This type of setup is referred to as quasi-static and has been found to be accurate because these small transients have little impact on the hydrodynamic interactions (Leong 2014; Perez et al. 2018).

Additionally, rather than creating a surrogate model for one specific UUV, this surrogate model is designed to account for different lengths and diameters of the UUV. This allows the

hydrodynamic interactions between different-size UUVs to be explored, rather than limiting the study to one UUV size. This enables better exploration of launch and recovery options and capabilities for different-size UUVs. The diameter of the UUV is nondimensionalized with the submarine diameter. This is called the submarine-to-UUV diameter ratio $D_{\text{Sub}}/D_{\text{UUV}}$. The length of the UUV is nondimensionalized by the diameter of the UUV and is known as the UUV length-to-diameter ratio L/D_{UUV}. All in all, the six inputs to the GP regression model are the longitudinal separation ratio, lateral separation ratio, UUV speed, UUV heading angle, submarine-to-UUV diameter ratio, and the UUV length-to-diameter ratio. The range of the parameters is chosen to reflect a realistic set of conditions (Table 1).

The surrogate ROM is trained on 100 CFD simulations at different locations within the domain. This data set comprises the **X** and **y** listed in equation (9). The locations of these specific CFD simulations are selected using active sampling. Active sampling is when each new data point is selected sequentially and at the location within the domain which provides the most improvement to the surrogate model (Sacks et al. 1989; Chaloner & Verdinelli 1995). The active sampling method for this study is the NonMyopic MultiFidelity (NMMF) sampling method (Hammond & Sapsis 2023). This approach utilizes the low cost of low-fidelity potential flow simulations to explore the domain and then provides the next optimally selected location for the high-fidelity CFD simulation. This NMMF sampling method is used because it allows for a more accurate surrogate model with a fewer number of CFD simulations (Hammond & Sapsis 2023). The surge, sway, and yaw force and moments are collected from each of the 100 CFD simulations. Each force or moment is used as its own distinct and separate **y** output, which is used to train three separate outputs for the surrogate model.

Overall, this surrogate takes the state vector, as well as the length and diameter of the UUV, and predicts the UUV surge, sway, and yaw body forces and moments due to the hydrodynamics interactions, which are denoted as X_s, Y_s, and N_s, respectively. This is performed by nondimensionalizing the state vector and UUV length to match the input variables in Table 1. These are then placed into $\mathbf{X}_*$ from equation (9), representing the location for which a prediction of the hydrodynamic interactions is desired. The 100 CFD simulation locations are organized into the data set **X** with three distinct labels **y**, one for each of the surge, sway, and yaw forces and moments. Equation (9) is then used to solve for the predicted surge, sway, and yaw body forces and moments due to the hydrodynamics interactions X_s, Y_s, and N_s. These ROM outputs are incorporated into the equations of motion by replacing the body forces with those predicted by the surrogate. Equation (11) shows the modified version of the simplified equations of motion that account for the hydrodynamic interactions.

Table 1 Input variable for hydrodynamic reduced order model

Symbol	Units	Bounds
R_{Long}	None	[−0.7, 0.7]
R_{Lat}	None	[0.059, 0.105]
u	Knots	[2, 5]
Ψ	Degrees	[−2, 2]
$D_{\text{Sub}}/D_{\text{UUV}}$	None	[5, 50]
L/D_{UUV}	None	[4.3, 13]

$$\begin{bmatrix} m - X_{\dot{u}} & 0 & 0 \\ 0 & m - Y_{\dot{v}} & -Y_{\dot{r}} \\ 0 & -N_{\dot{v}} & I_{zz} - N_{\dot{r}} \end{bmatrix} \begin{bmatrix} \dot{u} \\ \dot{v} \\ \dot{r} \end{bmatrix} = \begin{bmatrix} X_s + X_{\text{Prop}} \\ Y_s + Y_{uu\delta_r} u^2 \delta_r \\ N_s + N_{uu\delta_r} u^2 \delta_r \end{bmatrix} \tag{11}$$

Now that the hydrodynamic interactions surrogate model has been incorporated into the equations of motion, the UUV control system and autonomous behaviors can be analyzed to evaluate their robustness against these unwanted hydrodynamic interactions.

2.4. Control method

The pMarinePID app simulates the UUV PID controller. This app takes in the desired speed and heading from the pHelmIvP app and returns the input vector, which contains the propeller thrust X_{Prop} and rudder angle δ_r necessary to achieve the desired speed and heading. The thrust and rudder angle also depend on the current state of the vehicle. The difference between the desired and current state is known as the error, denoted as $e_u(t)$ and $e_\psi(t)$. The standard PID controller calculates the sum of some proportion of the error, its derivative, and integral as shown in equation (12) (Fossen 2011). The resulting $\tau_{X_{\text{Prop}}}$ and τ_{δ_r} represent the necessary change in thrust or rudder angle from the current state. These changes are added to the current thrust and rudder angle to determine new thrust $X_{\text{Prop},t+1}$ and rudder angle $\delta_{r,t+1}$ as outlined in equation (12).

$$\begin{aligned} e_u(t) &= u_d - u \\ e_\psi(t) &= \psi_d - \psi \\ \tau_{X_{\text{Prop}}} &= K_{p,X_{\text{Prop}}} e_u(t) + K_{d,X_{\text{Prop}}} e_u{}^{\cdot}(t) \\ &\quad + K_{i,X_{\text{Prop}}} \int_0^t e_u(\tau) d\tau \\ \tau_{\delta_r} &= K_{p,\delta_r} e_\psi(t) + K_{d,\delta_r} e_\psi{}^{\cdot}(t) \\ &\quad + K_{i,\delta_r} \int_0^t e_\psi(\tau) d\tau \\ X_{\text{Prop},t+1} &= X_{\text{Prop},t} + \tau_{X_{\text{Prop},t}} \\ \delta_{r,t+1} &= \delta_{r,t} + \tau_{\delta_{r,t}} \end{aligned} \tag{12}$$

Each of the K_p, K_d, and K_i constants are often referred to as gains and represent how much the proportional, derivative, and integral terms impact the change to the thrust or rudder angle. The thrust and rudder angles each have their own set of gains. These gains are determined for each vehicle in the study using the Ziegler Nichols method (Ellis 2012). Ultimately, the pMarinePID app has the input of the desired speed and heading from the desired state vector $\mathbf{x_d}$ along with the UUV state vector **x**. The app returns the input vector u containing the new propeller thrust $X_{\text{Prop},t+1}$ and rudder angle $\delta_{r,t+1}$.

2.5. Autonomous behaviors

2.5.1. Waypoints behavior The autonomous behavior of the UUV is modeled after the MOOS pHelm-IvP waypoint behavior (Benjamin et al. 2021). This waypoint behavior takes the current

state of the UUV and determines the desired speed and desired heading. In this study, the desired speed specified for a simulation is held constant. However, the desired heading is determined by establishing a series of waypoints, or locations, that the UUV will pass through. Once the UUV passes through a waypoint, it maneuvers toward the next waypoint. An imaginary track-line is established between the previous waypoint and the next waypoint. A perpendicular line between the UUV and the track-line is established. Once this perpendicular intersection point on the track-line is known, a lead point is determined by finding the point at a predetermined distance from the perpendicular intersection point on the track-line in the direction of the next waypoint. This distance is known as the lead distance d_{lead}. The desired heading is then computed by determining the heading of the lead point with respect to the UUV so that the UUV always desires to head toward the lead point. If the lead point extends beyond the next waypoint, the next waypoint becomes the lead point. Figure 3 illustrates the waypoints behavior.

The waypoints behavior is simulated in the pHelmIvP app. In summary, the pHelmIvP app, which uses the waypoints behavior, takes the state vector of the UUV at a given point $\mathbf{x_t}$ as an input and returns the desired state vector $\mathbf{x_{d,t}}$ containing the desired speed and desired heading. This desired state vector is fed into the pMarinePID app which uses control theory to determine the input vector $\mathbf{u_t}$ containing the appropriate propeller thrust and rudder angle. This input vector is then fed to the uSimMarine app which uses the equations of motion to determine a new UUV state vector $\mathbf{x_{t+1}}$. This loop is iterated along a small time step Δt to simulate the UUV motion. This process is summarized in Fig. 2.

By incorporating the GP surrogate model into the equations of motion as shown in equation (11), a simulation can be performed that accounts for the submarine and UUV hydrodynamic interactions. Figure 4 provides an example simulation of a large UUV performing a simple overtaking maneuver near the stern of the submarine with an overtaking velocity of $U_{\text{ot}} = 0.25\,\text{m/sec}$ and a submarine velocity of $U_{\text{sub}} = 1.5\,\text{m/sec}$ ($\sim$3 knots).

As the UUV approaches the stern of the submarine, the sway and yaw hydrodynamic interactions cause the UUV to be pulled and rotated toward the submarine which ultimately results in a collision. As the UUV starts to be pulled off course, it responds by positioning the rudder to maneuver the UUV away from the submarine. However, the standard behavior is not responsive enough to overcome these hydrodynamic interactions which ultimately results in a collision.

2.5.2. N_{uv} compensation The GP regression surrogate model is capable of determining the hydrodynamic interaction forces and moments in real time. This real-time modeling enables the hydrodynamic interactions to be incorporated into the equations of motion to determine how a UUV responds to these unwanted forces and moments. Additionally, this real-time modeling capability can be incorporated into the autonomous behaviors of the UUVs. If the UUV can anticipate the unwanted hydrodynamic forces and moments, new autonomous behaviors may be developed that determine a new desired heading and speed capable of better overcoming the hydrodynamic interactions and staying on course.

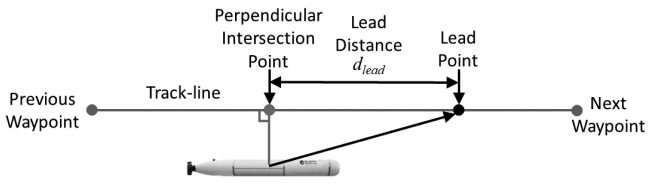

Fig. 3 Waypoints behavior: the purpose of this behavior is to traverse a set of waypoints along a track-line. The vehicle steers toward the lead point on the track-line rather than toward the next waypoint

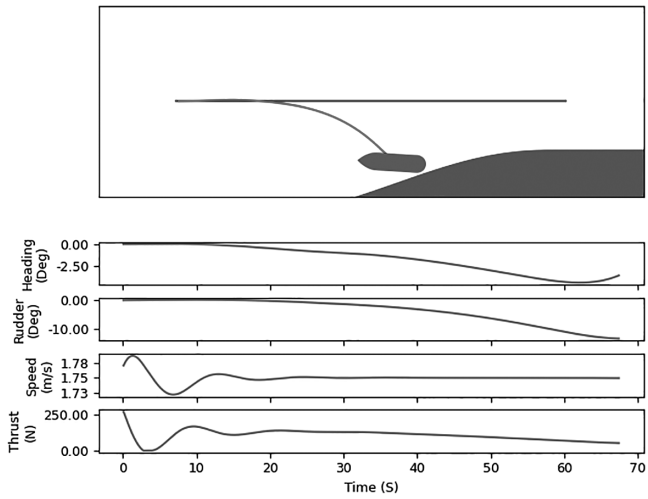

Fig. 4 The large UUV is unable to overcome the hydrodynamic interactions near the stern of the submarine which results in a collision

Figure 4 shows how the UUV is not responsive enough to overcome the hydrodynamic interactions between the submarine and UUV, which results in a collision. The UUV is inherently reactive because it only begins to course correct after it is pulled away from the track-line. By the time the UUV begins to stray significantly from the track-line, the standard waypoints behavior and UUV control system do not produce a strong enough response to prevent a collision. Rather than being reactive to the hydrodynamic interactions, the autonomous behavior can be altered to be proactive. Because the surrogate model is capable of predicting the hydrodynamic interaction forces and moments based on the current state of the UUV, the forces and moments can be anticipated before waiting for the UUV to stray off course and then try to recover.

In order to allow the UUV to anticipate hydrodynamic interactions, the GP surrogate model is integrated into the pHelmIvP app. This app simulates the autonomous behavior and is responsible for computing the desired speed and heading of the UUV. The GP surrogate model computes the predicted hydrodynamic interaction surge, sway, and yaw forces and moments on the vehicle based on its current state. If the UUV knows what hydrodynamic interaction forces and moments it will experience, it can adjust its desired speed and/or heading appropriately to stay on course. This enables the desired heading or desired speed to take into account the predicted impact of these forces and moments and keep the UUV on course.

Because there are multiple hydrodynamic interaction forces and moments acting on the UUV, there is no single UUV state that can offset all of these surges, sway, and yaw forces and moments at the same time. Additionally, there are multiple ways

in which the GP model could be incorporated into the autonomous behavior of the UUV. After exploring which of these forces or moments has the largest impact on the ability of the UUV to stay a course, the surge force is consistently the least influential force while the yaw moment has the largest influence. The best case found for which the UUV could overcome the hydrodynamic interactions and stay on course is by adjusting the desired heading to offset the hydrodynamic interaction yaw moment. The scheme by which this offset is determined will be referred to as N_{uv} compensation. This scheme is founded on the concept of the munk moment. The munk moment is a destabilizing moment experienced by a UUV in steady translation. When the flow is at a slight angle from the forward direction of the vehicle and this results in a munk moment (Fossen 2011; Newman 2017). This moment is destabilizing because the resulting munk moment will cause the UUV to want to rotate away from being parallel with the flow. This destabilizing moment usually means that a long slender object, like a UUV, is only stable when moving with its broadside to the flow. As such, the control surfaces are necessary to keep a UUV directionally stable.

The idea behind N_{uv} compensation is to place the UUV in such a desired state that the yaw moment of the UUV in this state offsets the hydrodynamic interaction yaw moment predicted by the GP model N_s at this location near the submarine. This means that a new compensated desired heading needs to be determined. This is found by using the N_{uv} coefficient of the UUV to solve for a compensated desired heading angle $\psi_{d,\text{comp}}$. This is achieved by first solving for a theoretical compensated sway velocity v_{comp} and then determining the theoretical heading angle that would produce this sway velocity. The derivation of this compensated desired heading angle is as follows

$$\begin{aligned} \gamma N_s &= N_{uv} u_d v_{\text{comp}} \\ \therefore v_{\text{comp}} &= \frac{\gamma N_s}{N_{uv} u_d} \\ \Delta\psi &= \tan^{-1}\left(\frac{u_d}{v_{\text{comp}}}\right) = \tan^{-1}\left(\frac{\gamma N_s}{N_{uv} u_d^2}\right) \\ \psi_{d,\text{comp}} &= \psi_d + \Delta\psi \end{aligned} \tag{13}$$

where γ is a factor that can be tuned as necessary and u_d and ψ_d are the outputs from the waypoints behavior of the pHelmIvP app. Figure 5 is the same simulation setup as Fig. 4, except that the UUV is now using N_{uv} compensation with $\gamma = 1$.

By using N_{uv} compensation, the UUV adjusts the desired heading to be rotated farther away from the submarine. This overcomes the hydrodynamic interaction that wants to rotate the bow of the UUV toward the submarine. Because N_{uv} compensation anticipates this hydrodynamic interaction, the UUV is able to overcome it and avoid the impending collision illustrated in Fig. 4.

2.5.3. Modified waypoints behavior The standard waypoints behavior establishes the inertial reference frame as an earth-fixed coordinate system. However, in order to study the hydrodynamic interactions between a submarine and UUV, the inertial reference frame is fixed to the center of buoyancy of the submarine. Because the submarine is constantly moving to maintain flow across the control surfaces in order to stay in control, the waypoints are not fixed to the earth and have a significant flow through them. This submarine velocity U_{sub} has a significant impact on the UUV as it tries to navigate to a waypoint. This is

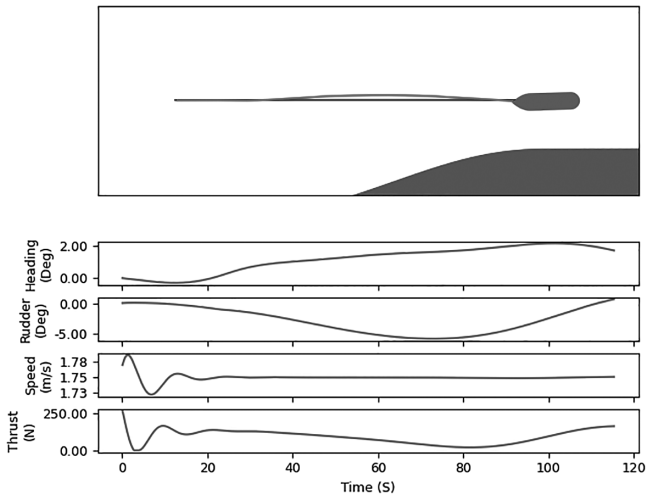

Fig. 5 Due to the N_{uv} compensation, the large UUV is now able to anticipate and overcome the hydrodynamic interactions near the stern of the submarine and avoid the impending collision seen in Fig. 4

analogous to having an earth-fixed waypoint with a strong current passing through it. The standard waypoint behavior is not designed to handle a significant current passing through a waypoint. In the event that the track-line is parallel to U_{sub}, like in an overtaking maneuver, the standard waypoint behavior performs well. However, when there is flow that crosses the track-line, the UUV is taken way off course. Figure 6 illustrates how a UUV behaves near a submarine moving forward. The blue line is the track-line between waypoints while the red line tracks the position of the UUV over time. Initially, the UUV is traveling parallel to the submarine. As the UUV desires to head down along the vertical track-line, it changes its heading to a maximum of about 60 degrees toward the submarine to advance toward the next waypoint. When the UUV is at this heading, the large cross flow causes the UUV

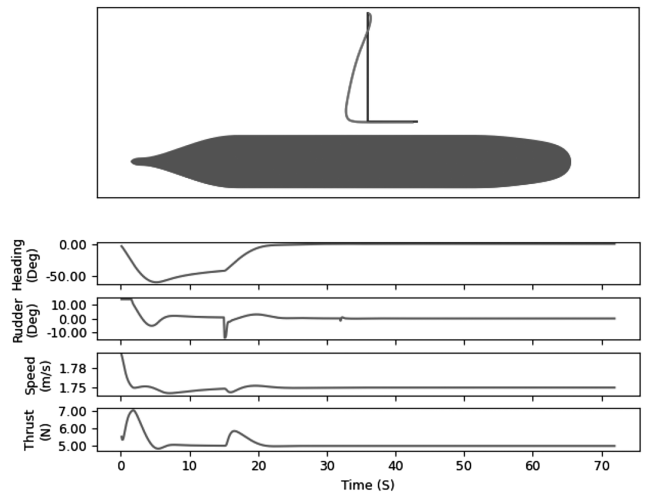

Fig. 6 Demonstration of the standard waypoints behavior with a moving submarine. The large cross flow pushes the UUV off course when not moving parallel to the submarine

to get pushed significantly off of the track-line. When the track-line is parallel to U_{sub}, the UUV is able to stay on the track-line.

This problem is addressed by creating a modified waypoint behavior. The modified waypoint behavior adjusts the position of the lead point based on the submarine speed. This can also be thought of in an earth-fixed coordinate system as adjusting the lead point based on a known constant current through the waypoints. Rather than place the lead point on the track-line at d_{lead} from the perpendicular intersection point, a new position is calculated for the lead point. This location is calculated by moving the lead point by d_{lead} from the perpendicular intersection point in the direction of U_{sub}. Additionally, the lead point is moved in the direction perpendicular to U_{sub} towards the next waypoint by a distance known as the lead offset d_{off}. Figure 7 shows how the lead point is determined. The angle between U_{sub} and the track-line is denoted as β.

This lead offset d_{off} is determined using equation (14)

$$d_{\text{off}} = \frac{\alpha d_{\text{lead}} U_{\text{ot}} \sin(\beta)}{U_{\text{sub}}} \tag{14}$$

where α is a parameter between zero and one that specifies how quickly the UUV transverses the track-line in the direction perpendicular to the cross flow. Also, recall that the relative speed between the UUV and submarine is denoted as $U_{\text{ot}} = U_{\text{UUV}} - U_{\text{sub}}$.

While modifying the position of the lead point appropriately adjusts the desired heading, it does not account for the desired speed of the UUV and fails to allow the UUV to accelerate or decelerate to follow the track-line. This ability was added by developing a speed policy behavior for the UUV where the speed policy correction factor is denoted as ϵ in equation (15).

$$U_{\text{UUV}} = U_{\text{sub}} + U_{\text{ot}} \cos(\beta) + \epsilon \tag{15}$$

If the UUV lags behind the track-line in the direction of U_{sub}, then the U_{UUV} increases. If the UUV leads the track-line, U_{UUV} decreases. The amount by which the U_{UUV} is adjusted is the speed policy correction factor ϵ, which is outlined in equation (15). The ϵ is established according to the U_{ot}, the length of the UUV L_{UUV}, and the distance between the UUV and the perpendicular intersection point d_{perp}. The policy is analogous to a saturated proportional gain and is set such that the maximum ϵ is achieved when the UUV lags the track-line in the direction of U_{sub} by a distance

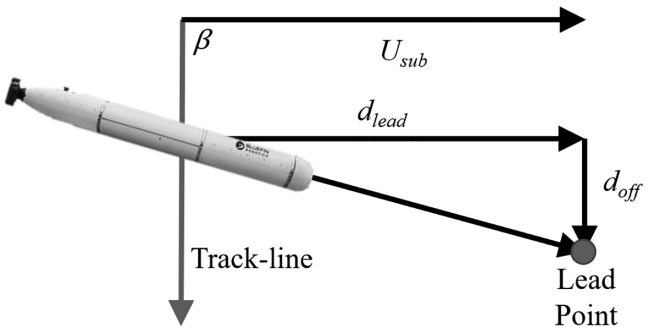

Fig. 7 Modified waypoints behavior: the position of the lead point is changed from the standard waypoint behavior. This enables the UUV to stay on the track-line despite having a large cross flow that overwhelms the standard waypoint behavior

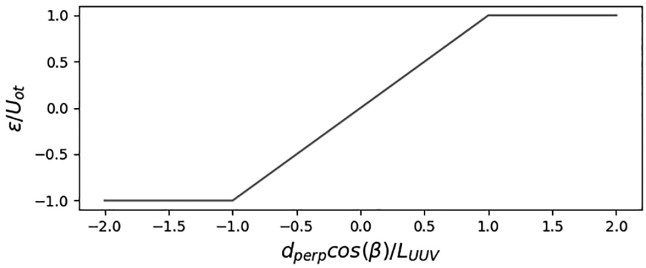

Fig. 8 Speed policy: This policy shown in nondimensional terms allows the UUV to accelerate or decelerate when the cross flow causes the UUV to fall behind or overshoot the track-line

of L_{UUV}. Figure 8 shows this nondimensionalized speed policy correction factor.

In order to compare the standard and the modified waypoints behavior, a test simulation is conducted for a small UUV, which is the REMUS 100 in this case. The course is to maneuver around a series of octagonally arranged waypoints with a U_{sub} of 1.5 m/sec ($\sim$3 knots), U_{ot} of 0.25 m/sec, and α of 1. Figure 9 shows a comparison of the standard and modified waypoints behavior.

The standard waypoints behavior is significantly affected by the cross-flow. The simulation using the standard waypoints behavior even resulted in the UUV missing one of the waypoints and having to circle back and get it. However, the modified waypoints behavior shows how the UUV is able to account for the cross flow and stay on its track-line. The UUV only needs to orient between ± 10 degrees in order to utilize the cross flow to move laterally. This approach prevents the UUV from experiencing the large strays seen by the standard waypoints behavior.

2.5.4. Robustness The main reason for implementing a UUV control system is to allow it to make course corrections from perturbations that take the UUV off course. In addition to the hydrodynamic interactions, there are other sources of perturbation that exist when a UUV is maneuvering. Determining the robustness of the UUV against these perturbations is vital to assess the feasibility of launch and recovery operations. Large-scale perturbations due to ocean eddies and currents occur at large enough time scales and length scales that they do not have a large impact on UUV launch and recovery operations (Adcroft et al. 2019). If a submarine and UUV are operating in an ocean cross current, over time they will drift with the current. Any changes to the current are slow enough and over large length scales that they will not have a large impact on UUV maneuverability. Likewise, small-scale turbulence caused by the vehicles moving through the water will have small enough time and length scales that they will not impact UUV motion (Osborn & Lueck 1985). However, the perturbations caused by surface waves are in the time and length scales that may have large impacts on UUV maneuverability.

Ocean waves are often described as being stochastic, meaning that they are random or unpredictable. These waves can be considered stochastic in terms of their amplitude or wave height. The height of ocean waves can vary widely, depending on wind speed, the distance over which the wind blows on the wave, and the sea state of the ocean surface. Ocean waves can also be considered stochastic in terms of their period, or time between waves. Due to this stochastic nature, waves are often described using probability distribution functions or wave spectra. As such, ocean waves are

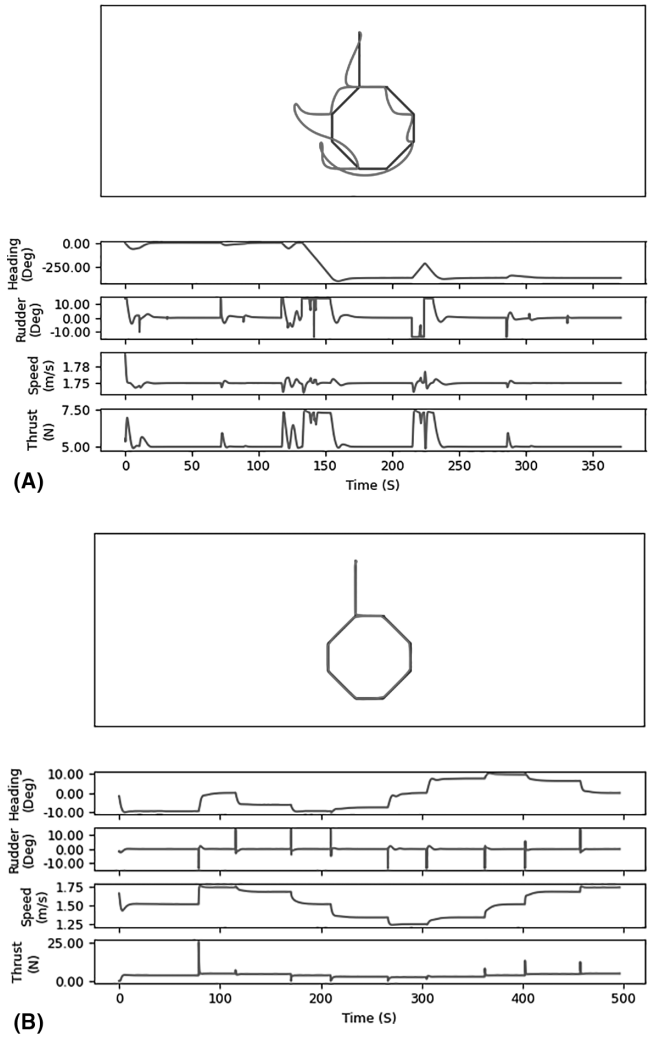

Fig. 9 Comparison of standard and modified waypoints behavior. Unlike the standard waypoints behavior, the modified waypoint behavior enables the UUV to stay on course across all course trajectories despite the large cross flow. (A) Standard waypoints behavior: this behavior is not resistant to the cross flow. This causes the UUV to be pushed off course and even get turned around. (B) Modified waypoints behavior: this behavior is resistant to the cross flow, even at all of the different course trajectories

often categorized into different sea states as shown in Table 2 (McCreight 1998).

The solution space of the impact of waves on different combinations of UUV size, location, speed, heading, and depth is very large. In order to fully explore this solution space and develop operating envelopes, a large number of UUV simulations needs to be performed. If the waves are modeled as a probability distribution function or spectra, then the impact of the waves on the motion of the UUV is also probabilistic. Implementing the waves in this matter is complex and computationally expensive. Ultimately, the results need to be simplified to a nonprobabilistic representation when developing operating envelopes. As such, the waves are implemented in a deterministic manner and modeled as a plane progressive wave using linear wave potential theory.

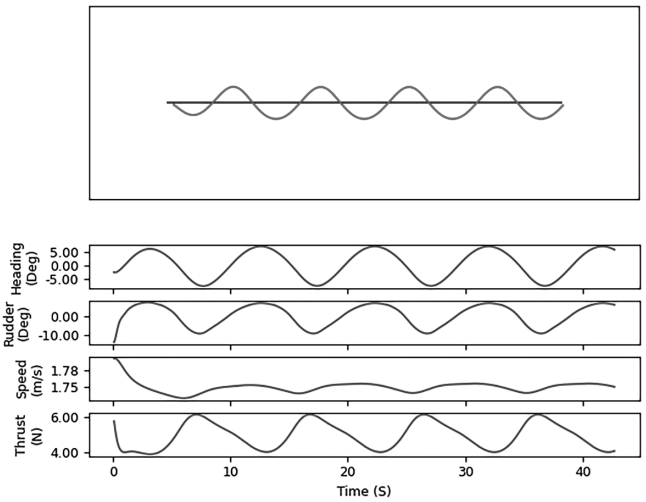

Fig. 10 A small UUV in sea state 5 at 50 m deep is pushed by the waves and oscillates around the track-line

Modeling the waves in this way is common and is also often considered as having the greatest practical significance (Newman 2017). This is cheaper and easier to implement and allows for the creation of simpler operating envelopes.

The 2D fluid velocity components due to the waves are defined as u_w and v_w (Newman 2017). These fluid velocities are in the inertial coordinate system where u_v is in the direction in which the wave is progressing and v_w is in the direction pointed down toward deeper depths. The significant wave height is defined as the average of the highest 1/3 of the wave heights over a time history. The amplitude A of a wave is 1/2 of the wave height. As such, A is set for each sea state as 1/2 of the largest value in the range of significant wave heights listed in Table 2 in order to be conservative. The angular frequency $\omega = 2\pi/T$ is also found for each sea state using the most probable period. The wave number $k = 2\pi/\lambda$ is found using the wave length λ.

The wave length λ depends on the angular frequency ω of the wave, as well as the dispersion relationship, which depends on the depth to the ocean floor. In this case, the deep water assumption is made meaning that the ocean floor is deeper than $\lambda/2$. This is a safe assumption given the range of possible wavelengths and the requirements for the minimum charted depth of water (NATO 2002). This means the dispersion relationship is $k = \omega^2/g$ and the wave length is found using $\lambda = g\omega^2/(2\pi)$ where g is the acceleration due to gravity. Lastly, x and y represent the location in the flow field where y is the depth.

$$u_w = \omega A e^{ky} \cos(kx - \omega t) \tag{16}$$

Table 2 Sea state table for the general North Atlantic

Sea state	Significant wave height (m)	Period range (s)	Most probable period (s)
0–1	0–0.1	–	–
2	0.1–0.5	3.3–12.8	7.5
3	0.5–1.25	5.0–14.8	7.5
4	1.25–2.5	6.1–15.2	8.8
5	2.5–4.0	8.3–15.5	9.7
6	4.0–6.0	9.8–16.2	12.4

$$v_w = \omega A e^{ky} \sin(kx - \omega t) \tag{17}$$

This flow field is ultimately incorporated into the UUV simulator by converting the flow field into the UUV body-fixed coordinate system and then combining the UUV velocities with these velocities due to the waves from equations (16) and (17). Figure 10 is an example illustration of a small UUV traversing a 10 m trackline operating 50 m deep in sea state 5 conditions. The UUV is operating at 1.75 m/sec (~3.5 knots) with the inertial frame moving 3 knots, meaning $U_{ot} = 0.25$ m/sec.

In this high sea state, the UUV is pushed off course by the wave flow field even at 50 m deep. The autonomous behavior and control system allows for the UUV to course correct, but the waves repeatedly push the UUV off course.

The UUV simulator only uses three degrees of freedom. In order to be conservative, the perturbations caused by the waves are assumed to be in the same plane as the UUV velocities. This causes the UUV to be pushed toward or away from the submarine. This is a conservative approach because it models the worst-case scenario of the direction of fluid velocities due to the wave. This would be analogous to having a UUV operate above a submarine. The waves would push it up or down toward the submarine. If the UUV were to the side of the submarine, these perturbations would cause the UUV to move in a direction orthogonal to the plane between the vehicle axes. Additionally, the submarine is assumed to have no impact on damping the fluid velocity due to the waves. This assumption is made for ease of implementation, but it is a conservative approach representing a worst-case scenario.

2.6. UUV simulation setup

This study examined three different UUV sizes: small, medium, and large. The small UUV uses the inertial properties and hydrodynamic coefficients of the Remus 100 (Prestero 2001). The medium and large UUVs use the corresponding inertial properties and hydrodynamic coefficients of the Naval Postgraduate School (NPS) Autonomous Underwater Vehicle (AUV) II and the Swimmer Delivery Vehicle, respectively (Warner 1991; Healey & Lienard 1993; Fossen 2011). The submarine in this simulation is the Defense Advanced Research Projects Agency SUBOFF hull that has been scaled up to have a diameter of 34 feet (10.363 m) (Groves et al. 1989). The submarine was simulated at speeds between two and five knots. This is based on the minimum speed for controllability of a submarine and the maximum speed of several UUVs (Fedor 2009).

2.7. UUV simulation validation

The UUV simulator is validated against UUV experimental runs to ensure that it is accurately reflecting the real-world physics (Warner 1991; Prestero 2001). An experiment of a Remus 100 UUV performing a step change in rudder angle of four degrees found that the resulting yaw rate was about −10 degrees per second (Prestero 2001). The UUV simulator predicted a yaw rate of −10.04 degrees per second. Similarly, an experiment on the NPS AUV II was performed using rudder commands that alternated by ±15 degrees every 45 seconds (Warner 1991). These rudder commands resulted in a yaw rate of about ±7.5 degrees per second. The UUV simulator predicted a yaw rate of about ±7.24 degrees per second. This demonstrates that the UUV simulator is able to replicate the results experienced by real-world UUVs.

3. Results

3.1. Force and moment maps

The GP regression surrogate model shows that the regions with the largest hydrodynamic interactions are near the bow and stern of the submarine (Hammond & Sapsis 2023). When a UUV operates in these regions, there is a high risk of collision. Figure 11 shows the nondimensional hydrodynamic interaction sway and yaw coefficients Y'_s and N'_s experienced by the UUV in various locations around the submarine. A negative sway and yaw cause the

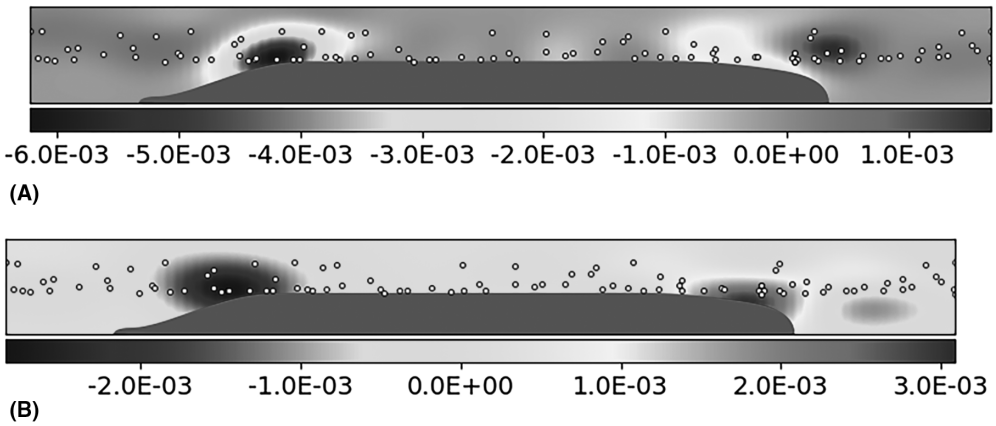

Fig. 11 Colormaps of the hydrodynamic interaction sway and yaw coefficients Y'_s and N'_s at different lateral and longitudinal positions with respect to the submarine. The dots represent the locations of a CFD simulation (Hammond & Sapsis 2023). (A) Colormap of sway coefficient Y'_s at various locations around the submarine at a fixed $U = 3.5$ knots, $\phi = 0^\circ$, $D_{Sub}/D_{UUV} = 10$, and $L/D_{UUV} = 8$. Regions around the bow of the submarine push the UUV away from the submarine while regions around the stern of the submarine pull the UUV toward the submarine. (B) Colormap of yaw coefficient N'_s at a fixed $U = 3.5$ knots, $\phi = 0^\circ$, $D_{Sub}/D_{UUV} = 10$, and $L/D_{UUV} = 8$. Regions around the bow of the submarine rotate the bow of the UUV away from the submarine while regions around the stern of the submarine rotate the UUV bow toward the submarine

UUV to be sucked toward and the UUV bow to be rotated toward the submarine respectively. This figure is for a large UUV which is one meter in diameter and 8 m long traveling at 1.75 m/sec (~3.5 knots) parallel to the submarine. The surrogate model is capable of altering these additional parameters and generating new maps, but the added dimensionality is not shown in order to be concise and simply illustrate regions with large hydrodynamic interactions.

3.2. Results for standard UUV

Due to the low cost of running the GP surrogate model, many simulations may be performed in various regions around the submarine and under various conditions. This allows for the creation of a safe operating envelope, a region under specified conditions in which the UUV is capable of overcoming the hydrodynamic interactions. Likewise, a region can be identified in which a collision is predicted. A close call is defined as a case in which the UUV comes within one UUV diameter of the submarine without a collision, or when the UUV is directly in front of or behind the submarine. A large stray is defined as the case when the hydrodynamic interactions cause the UUV to stray away from its track-line by more than 1 m. Figure 12 illustrates the operating envelope for the small, medium, and large UUV that are traveling at the same speed as the submarine at $U_{sub} = 1.5$ m/sec (~3 knots) with $d_{lead} = 3L_{UUV}$ and no waves. Figure 12 shows that all three of the UUVs have issues overcoming the hydrodynamic interactions illustrated in Fig. 11. All three different size UUVs have large operating regions near the stern of the submarine that result in collisions. Additionally, the large hydrodynamic interactions near the bow of the submarine because all three size UUVs to stray large distances from the track-line, even though they do not result in a collision with the submarine. This means that UUVs operating with the standard waypoint behavior will struggle to perform overtaking maneuvers without experiencing large strays or collisions. As such, launch and recovery architectures and schemes may be more successful if implementing a lateral approach to the parallel midbody section of the submarine.

There are several parameters, such as U_{ot}, U_{sub}, and d_{lead}, which have an influence on how the hydrodynamic interactions impact the UUV. As such, many more operating envelopes could be created for a range of different scenarios. However, after sampling several different scenarios, varying the U_{ot} and U_{sub} had a very small impact on the operating envelope compared to d_{lead}. This is likely because U_{ot} and U_{sub} have narrow ranges for launch and recovery operations and the vehicle maneuverability is relatively constant over this range. However, d_{lead} influences the vehicle behavior, rather than making small adjustments to the underlying physical simulation setup. Figure 13 shows how different values of d_{lead} influence the operating envelope for the small UUV. These operating envelopes are for UUVs at the same speed as the submarine at $U_{sub} = 1.5$ m/sec (~3 knots) and no waves, just like Fig. 12.

As the d_{lead} decreases, the unsafe regions around the submarine decrease in size. Placing the lead point closer to the UUV allows the UUV to more aggressively pursue the track-line, perform better against the hydrodynamic interactions, and expand the safe operating region. This trend also exists for medium and large UUVs. However, the unsafe regions are still large enough to present problems with launch and recovery operations especially if overtaking maneuvers are involved. Adjusting d_{lead} alone is not enough to overcome the hydrodynamic interactions.

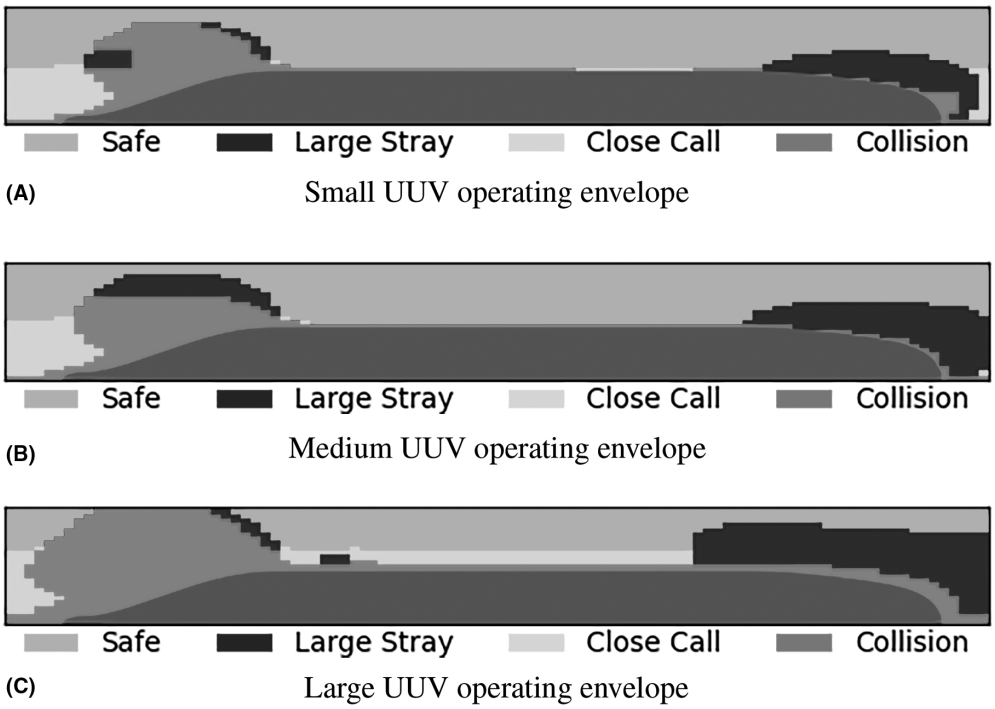

Fig. 12 Operating envelope for the small, medium, and large UUVs that are traveling at the same speed as the submarine at $U_{sub} = 1.5$ m/sec (~3 knots) with $d_{lead} = 3L_{UUV}$ and no waves. (A) Small UUV operating envelope. (B) Medium UUV operating envelope. (C) Large UUV operating envelope

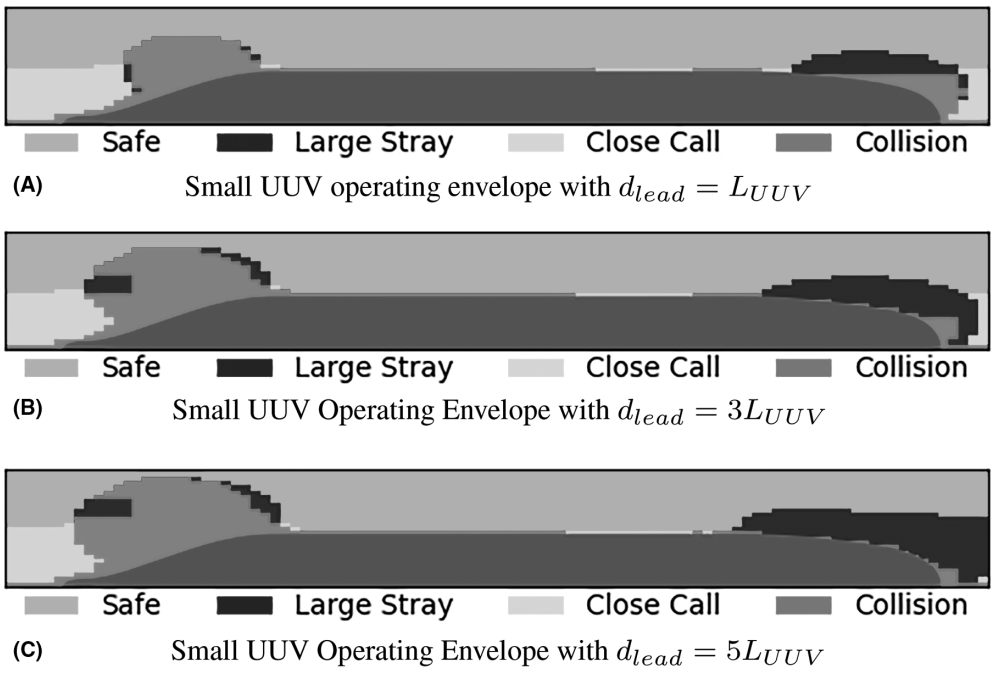

Fig. 13 Impact of d_{lead} on the operating envelopes for the small UUV traveling at the same speed as the submarine at $U_{\text{sub}} = 1.5$ m/sec (~3 knots) with no waves. A smaller d_{lead} results in larger safe operating envelopes. (A) Small UUV operating envelope with $d_{\text{lead}} = L_{\text{UUV}}$. (B) Small UUV operating envelope with $d_{\text{lead}} = 3L_{\text{UUV}}$. (C) Small UUV operating envelope with $d_{\text{lead}} = 5L_{\text{UUV}}$

3.3. Results for N_{uv} compensated UUV

As discussed previously, N_{uv} compensation is a method by which the GP surrogate model of the hydrodynamic interactions is used to influence the UUV autonomous behavior by determining a new heading angle $\psi_{d,\text{comp}}$ that compensates for the hydrodynamic interactions. Figure 5 provides an example of how this N_{uv} compensation is able to allow the UUV to account for and overcome the hydrodynamic interactions. This results in the UUV staying on track and avoiding the impending collision with the submarine.

This approach also enables the N_{uv} compensation to be simulated very rapidly for UUVs at various locations around the submarine, which allows for the development of new operating envelopes. Figure 14 represents the new N_{uv} compensated operating envelopes. These are for UUVs at the same speed as the submarine at $U_{\text{sub}} = 1.5$ m/sec (~3 knots) with $d_{\text{lead}} = 3L_{\text{UUV}}$ and no waves, just like Fig. 12.

The use of N_{uv} compensation drastically reduces the collision and large stray regions for the UUVs compared to Fig. 12. This N_{uv} compensation also provides a significant increase to the size of the safe operating regions compared to changing the d_{lead}. This demonstrates the effectiveness of the N_{uv} compensation to anticipate the hydrodynamic interactions and to appropriately adjust the desired heading angle. The N_{uv} compensation outlined in equation (13) is especially beneficial for the medium and large UUVs. This is largely because of the common square-cube law. This law states that the forces and moments experienced by the UUVs increase in proportion to the surface area, or square of the characteristic length. However, the mass and inertial properties of the UUV increase in proportion to the volume, or the cube of the characteristic length. As such, as a UUV becomes larger, its inertial properties increase faster than the forces and moments it experiences, so the vehicle is more resistant to accelerations. Also, there is no single UUV heading and speed that can balance all of the different hydrodynamic interactions acting on the vehicle. As such, the small UUV experiences larger deviations from its course due to the other uncompensated hydrodynamic interactions when compared to the larger UUVs. Larger UUVs have enough inertia to be resistant to these uncompensated forces.

In equation (13), the γ parameter is present to allow for the tuning of the N_{uv} compensation. If the moment from the N_{uv} exactly offsets the moment predicted by the GP surrogate N_s, then $\gamma = 1$. For the medium and large UUVs, $\gamma = 1$ works very well. However, for the small UUV with smaller inertial properties, this value is too low. The new compensated heading angle is not aggressive enough to overcome the hydrodynamic interactions. However, by selecting a γ that is too large, the UUV is too aggressive and overcorrects from the hydrodynamic interactions. The following figure illustrates the impact of γ on the compensated operating envelope of the small UUV.

Figure 15 shows how the N_{uv} compensated small UUV with $\gamma = 1$ has a smaller safe operating region than when $\gamma = 5$. However, when the parameter is increased to $\gamma = 10$, the vehicle overcorrects which reduces the safe operating envelope of the vehicle. As such, there is a γ for each vehicle which maximizes the size of the safe operating envelope.

Due to the square-cube law, the medium and large UUVs perform much better when the yaw moment from the hydrodynamic interaction surrogate N_s equals the yaw moment from the N_{uv} coefficient. This means that the γ values for these vehicles are much closer to one. The final values identified for γ for the small, medium, and large UUVs respectively are 5.22, 1.30, and 1.03. An empirical equation is developed to predict the γ parameter based on the combined mass and added mass M_{11} of the UUV

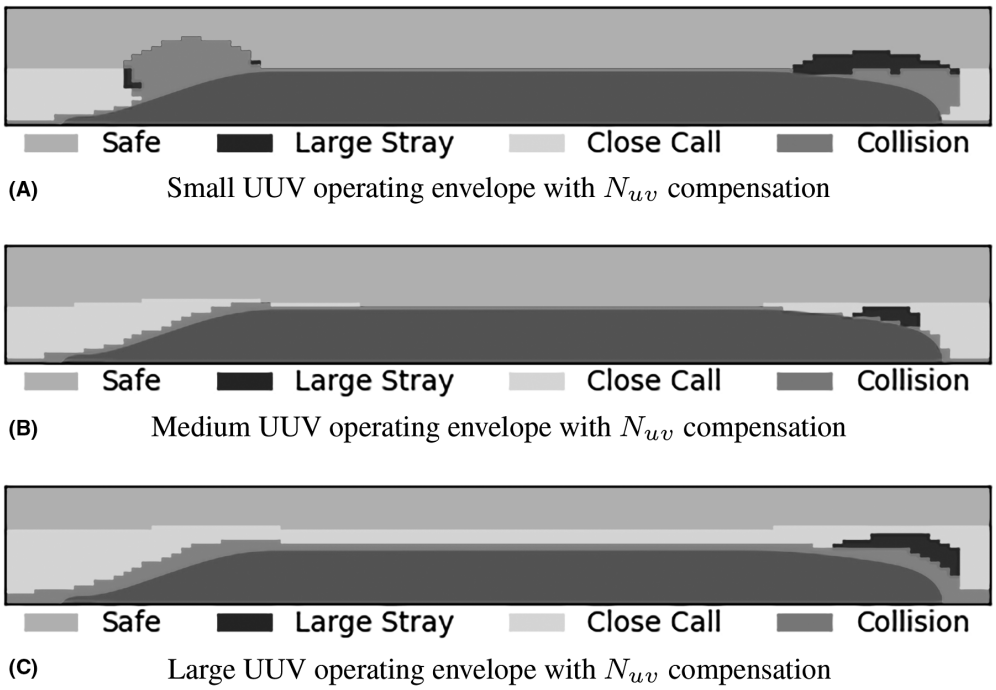

Fig. 14 N_{uv} compensated operating envelopes for the small, medium, and large UUVs that are traveling at the same speed as the submarine at $U_{sub} = 1.5$ m/sec (~3 knots) with $d_{lead} = 3L_{UUV}$ and no waves. The N_{uv} compensation increases the safe operating region around the submarine. (A) Small UUV operating envelope with N_{uv} compensation. (B) Medium UUV operating envelope with N_{uv} compensation. (C) Large UUV operating envelope with N_{uv} compensation

moving in the forward direction. This is the term in the first row and column of the inertial matrix M in equations (3) and (11). The values of M_{11} for the small, medium, and large UUVs are 33.6, 212.9, and 6020 kg, respectively. Equation (18) provides a means of determining γ based on the M_{11} term of the UUV.

$$\gamma(M_{11}) = 10^{4.538\left(\log_{10}(M_{11})\right)^{-4.364}} \tag{18}$$

Because these values of γ provided the largest safe regions in the operating envelopes, they are used as the default values throughout this study. This includes the operating envelopes in Fig. 14.

3.4. Effects of waves

Determining the robustness of the UUV against perturbations is important to the investigation of the UUV maneuvering capability during launch and recovery. Ocean waves provide the most applicable means of large perturbations experienced by the UUV. These perturbations caused by ocean waves are incorporated into the UUV motion simulator. In order to be conservative, these perturbations are assumed to be in the worse case direction that pushes the UUV toward or away from the submarine, rather than in an orthogonal direction. These perturbations also vary in magnitude based on the sea state and operating depth of the UUV. The following figure shows how the operating envelopes of the different size UUVs without N_{uv} compensation are affected by the ocean waves. The waves are sea state 6 and the UUV operating depth is 50 m. The lead distance is $d_{lead} = 3L_{UUV}$ just like Fig. 12.

When compared to the no-wave condition in Fig. 12, the safe operating envelope at sea state 6 at 50 m is drastically reduced. For the small UUV, the operating region that results in a collision with the submarine is very large and entirely encompasses the submarine. This drastically reduces the chance of a successful launch or recovery operation. The medium UUV also has an increase in the size of the collision regions around the submarine, but the remainder of the area results in large strays. This means that the medium UUV may not collide with the submarine but will stray by more than one meter from the track-line due to the waves. The large UUV has a reduction of the safe operating region compared to Fig. 12, but is much more robust to the wave perturbations than the smaller UUVs. This is a good demonstration of the square-cube law. Fortunately, sea states of 6 or above occur less than 27% of the time, and vessels try to avoid such rough seas so this case represents a relatively strong perturbation (Doerry 2008). Additionally, 50 m in depth is likely near the minimum depth at which launch and recovery operations will take place in order to maintain vertical separation from surface vessels (NATO 2002). However, UUV launch and recovery can be performed at deeper depths based on the maximum depth of the UUV in order to reduce the impact of the waves. The Remus 100 has a maximum rated depth of 100 m so operating below this is unfeasible. The following figure illustrates the same sea state 6 and other parameters as Fig. 16, but the UUV is now operating at a depth of 90 m.

Figure 17 shows a large increase in the safe operating regions for the small and medium size UUV compared to Fig. 16. By operating 40 m deeper, the waves have much less of an impact on the UUV motion and make the chances of successful launch or recovery much more likely.

Another way in which the safe operating envelope may be expanded is by providing N_{uv} compensation. By compensating the

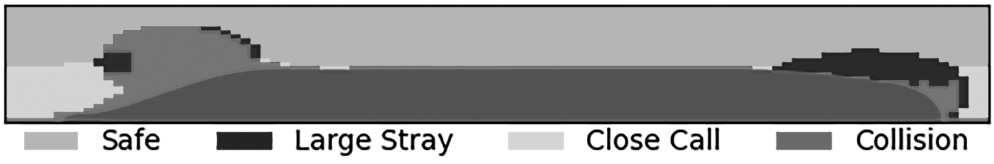

(A) N_{uv} compensation for small UUV with $\gamma = 1$

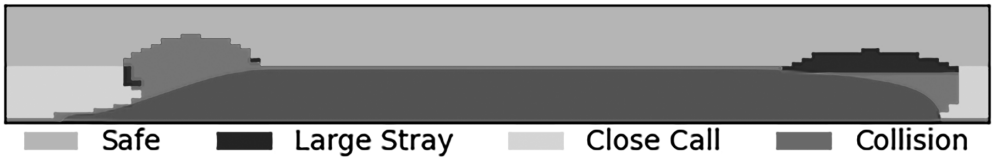

(B) N_{uv} compensation for small UUV with $\gamma = 5$

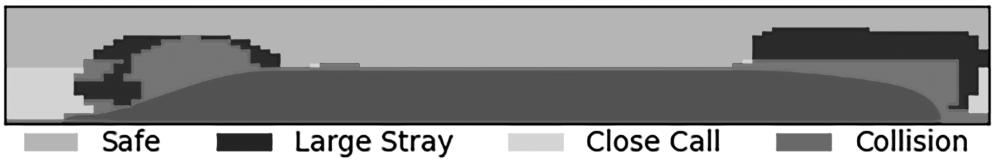

(C) N_{uv} compensation for small UUV with $\gamma = 10$

Fig. 15 Impact of γ on the N_{uv} compensated operating envelopes for a small UUV that is traveling at the same speed as the submarine at $U_{sub} = 1.5$ m/sec ($\sim$3 knots) with $d_{lead} = 3L_{UUV}$ and no waves. The γ parameter can cause the UUV to undercorrect and overcorrect for the hydrodynamic interactions. (A) N_{uv} compensation for small UUV with $\gamma = 1$. (B) N_{uv} compensation for small UUV with $\gamma = 5$. (C) N_{uv} compensation for small UUV with $\gamma = 10$

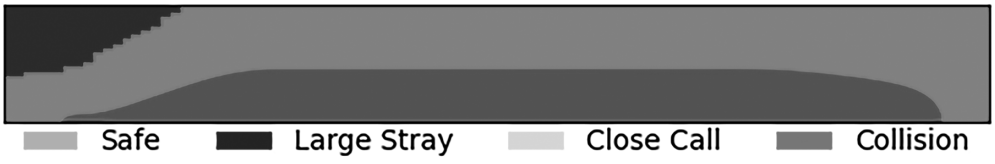

(A) Small UUV operating envelope without N_{uv} compensation in sea state 6 at 50 meters deep.

(B) Medium UUV operating envelope without N_{uv} compensation in sea state 6 at 50 meters deep.

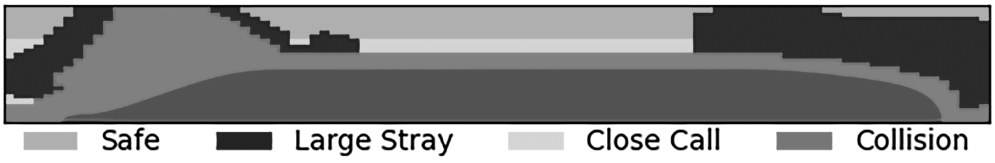

(C) Large UUV operating envelope without N_{uv} compensation in sea state 6 at 50 meters deep.

Fig. 16 Operating envelopes for different size UUVs without N_{uv} compensation in sea state 6 at a depth of 50 m. (A) Small UUV operating envelope without N_{uv} compensation in sea state 6 at 50 m deep. (B) Medium UUV operating envelope without N_{uv} compensation in sea state 6 at 50 m deep. (C) Large UUV operating envelope without N_{uv} compensation in sea state 6 at 50 m deep

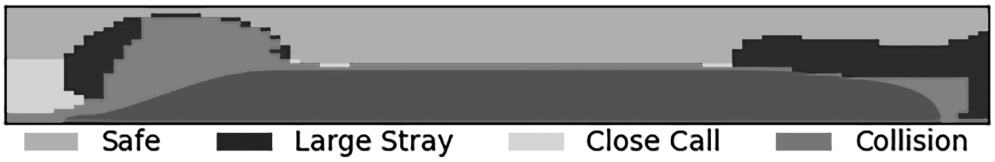

(A) Small UUV operating envelope without N_{uv} compensation in sea state 6 at 90 meters deep.

(B) Medium UUV operating envelope without N_{uv} compensation in sea state 6 at 90 meters deep.

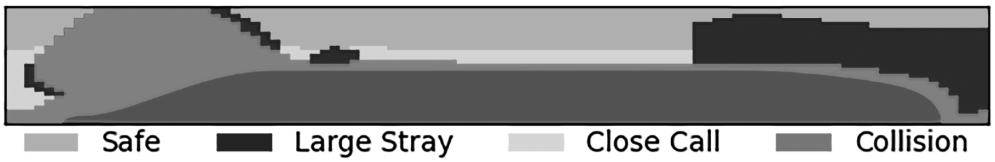

(C) Large UUV operating envelope without N_{uv} compensation in sea state 6 at 90 meters deep.

Fig. 17 Operating envelopes for different size UUVs without N_{uv} compensation in sea state 6 at a depth of 90 m. (A) Small UUV operating envelope without N_{uv} compensation in sea state 6 at 90 m deep. (B) Medium UUV operating envelope without N_{uv} compensation in sea state 6 at 90 m deep. (C) Large UUV operating envelope without N_{uv} compensation in sea state 6 at 90 m deep

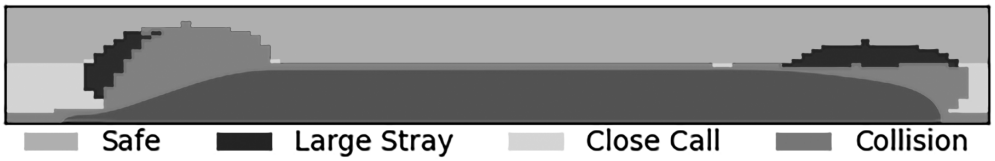

(A) Small UUV operating envelope *with* N_{uv} compensation in sea state 6 at 90 meters deep.

(B) Medium UUV operating envelope *with* N_{uv} compensation in sea state 6 at 90 meters deep.

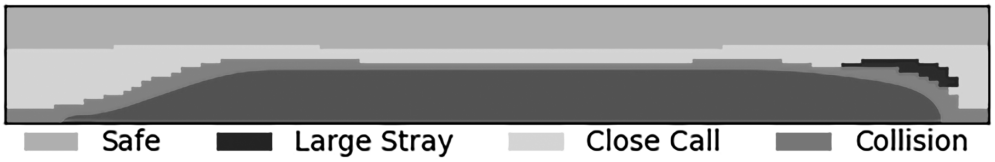

(C) Large UUV operating envelope *with* N_{uv} compensation in sea state 6 at 90 meters deep.

Fig. 18 Operating envelopes for different size UUVs with N_{uv} compensation in sea state 6 at a depth of 90 m. (A) Small UUV operating envelope with N_{uv} compensation in sea state 6 at 90 m deep. (B) Medium UUV operating envelope with N_{uv} compensation in sea state 6 at 90 m deep. (C) Large UUV operating envelope with N_{uv} compensation in sea state 6 at 90 m deep

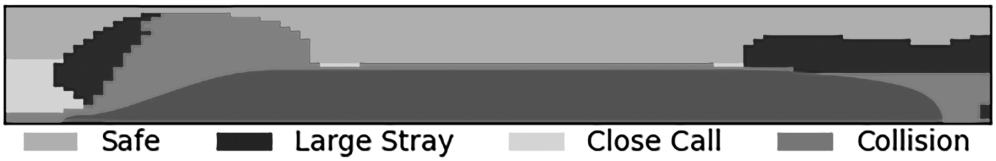

(A) Small UUV operating envelope without N_{uv} compensation in sea state 5 at 50 meters deep.

(B) Medium UUV operating envelope without N_{uv} compensation in sea state 5 at 50 meters deep.

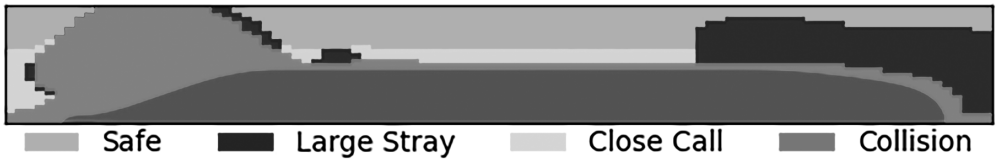

(C) Large UUV operating envelope without N_{uv} compensation in sea state 5 at 50 meters deep.

Fig. 19 Operating envelopes for different size UUVs without N_{uv} compensation in sea state 5 at a depth of 50 m. (A) Small UUV operating envelope without N_{uv} compensation in sea state 5 at 50 m deep. (B) Medium UUV operating envelope without N_{uv} compensation in sea state 5 at 50 m deep. (C) Large UUV operating envelope without N_{uv} compensation in sea state 5 at 50 m deep

desired heading for the anticipated hydrodynamic interactions, the UUV is better equipped to operate near the submarine. Figure 18 illustrates how providing N_{uv} compensation for the previous setup impacts the operating envelopes of Fig. 17.

By providing N_{uv} compensation, the safe operating envelopes are able to drastically increase in size for the medium and large UUV. The N_{uv} compensation provides an improvement in the operating envelope of the small UUV, but it still has regions near the bow and stern of the submarine which result in a collision, similar to Figs. 14 and 15. Again, this is due to the square-cube law.

At lower sea states, the UUVs are more capable of overcoming wave perturbations. Even at sea state 5 and 50 m deep, the operating envelopes of UUVs without N_{uv} are much better than those at sea state 6. Figure 19 shows the operating envelopes for the different size UUVs at sea state 5 and 50 m deep.

These operating envelopes look much more like the case with no waves in Fig. 12 than the case in sea state 6 at 50 m deep, especially for the small and medium UUVs. The UUVs are much more capable of overcoming these perturbations than those of sea state 6 at 50 m. The ocean waves are at sea state 5 or lower more than 73% of the time. Additionally, these operating envelopes can be improved by incorporating N_{uv} compensation, as seen when comparing Figs. 12 and 14 and also Figs. 17 and 18.

Overall, the UUV autonomous behaviors and control system are relatively robust to ocean waves. At the minimum likely operating depth for launch and recovery operations in sea state 5, the UUVs have similar operating envelopes as those with no waves. Once sea state 6 is reached, the small and medium UUV experience large strays or collisions, but this can be drastically mitigated by operating at lower depths where the impacts of the waves decay away. The N_{uv} compensation also provides improvements to the operating envelopes and demonstrates the same robustness against the ocean waves.

4. Conclusion

Determining the hydrodynamic interaction forces and moments between a UUV and submarine in real time is essential to simulate UUV motion during launch and recovery operations. Simplified potential flow simulators can be solved very quickly, but fail to capture the accurate physics of CFD simulations, which are too computationally expensive to be solved in real-time. A GP regression surrogate model is developed that is capable of predicting the UUV and submarine hydrodynamic interactions in real time. We develop a method to incorporate this GP surrogate model of the hydrodynamic interactions into a UUV motion simulator. This enables the use and evaluation of the UUV autonomous behavior and control system against the hydrodynamic interactions. Because this can be simulated rapidly, this allows for the creation of safe operating envelopes in which the UUV is capable of overcoming the hydrodynamic interactions. This simulation approach also enables the development of new UUV autonomous behaviors that incorporate the predicted hydrodynamic interactions. This provides modified desired headings and speed which improves the capability of the UUV to overcome the hydrodynamic interactions.

The simulations of how the hydrodynamic interactions impact the UUV motion show that there are regions near the bow and

stern of the submarine just beyond the parallel midbody section that result in large straying from the track-line or collisions between the two vehicles. These unsafe operating regions extend laterally from the bow and stern of the submarine so certain overtaking maneuvers may not be feasible with standard UUV autonomous behaviors. Also, lateral approaches prove problematic to standard UUV autonomous behaviors because they do not account for the moving inertial frame of the submarine so the UUV has large strays from the track-line. However, by modifying the UUV autonomous behavior, improvements are made to both problems of the moving inertial frame and the unsafe regions. The modified waypoints behavior provides a means of modifying the UUV desired heading and speed to account for the moving inertial frame and enable the UUV to stay on the track-line during a lateral approach. Also, the N_{uv} compensation allows the UUV to proactively account for the hydrodynamic interactions that it will experience. This improves the size of the safe operating region for the UUVs and better enables overtaking maneuvers. While waves provided perturbations that have the potential to be problematic, it is not until sea state 6 at the minimum likely depth of 50 m deep that these perturbations have a significant impact on the safe operating envelopes of the vehicles. Sea states of 5 or lower has little impact on the operating envelope at this depth. Also, at sea state 6, operating deeper around 90 m causes the UUV to experience significantly less impact from the waves so the safe operating envelope is comparable to that of lower sea states.

Increasing the complexity of the UUV simulator is left for future work. This may include modeling transient UUV behavior to account for a higher simulation degree of freedom or simulating the hydrodynamic interactions near a submarine appendage, like the sail or a dry deck shelter. Increasing the UUV simulation complexity or the number of degrees of freedom increases the input dimensions of the surrogate model that accounts for the hydrodynamic interactions. In order to fully account for all of the parameters in the UUV state vector, a quasi-static surrogate cannot be used. This means that the CFD simulations need to be unsteady rather than steady. This drastically increases the CFD simulation complexity, increases the simulation computational time, and increases the number of simulations needed to explore the domain. This may ultimately require more effective surrogate models such as those based on neural networks or operators (Pickering et al. 2022).

Acknowledgments

B.M.H. has been supported as a PhD student by the MIT 2N Navy Program. T.P.S. has been supported by the ONR Grants ONR – N00014-21-1-2357 and N00014-20-1-2366. Discussions with the following individuals and teams are also greatly appreciated.

- Chris Harding, Geoffrey McNally, and team: Warfare Integrated Systems Branch and Naval Undersea Warfare Center.
- Daniel Milligan and team: Undersea Vehicles Lead and General Dynamics Electric Boat.
- Joel Parry and team: Maritime Warfare and ISR, Business Area Lead, and Draper.
- Sasha Tsarev: Maritime Systems Hydromechanics Branch and Naval Surface Warfare Center.
- David A. Drazen: Chief Technology Officer and Naval Surface Warfare Center.
- CDR Kyle Weorner: Program Manager, Tactical Technology Office, and Defense Advanced Research Projects Agency.

References

Adcroft, A., Anderson, W., Balaji, V., Blanton, C., Bushuk, M., Dufour, C. O., Dunne, J. P., Griffies, S. M., Hallberg, R., Harrison, M. J., Held, I. M., Jansen, M. F., John, J. G., Krasting, J. P., Langenhorst, A. R., Legg, S., Liang, Z., McHugh, C., Radhakrishnan, A., Reichl, B. G., Rosati, T., Samuels, B. L., Shao, A., Stouffer, R., Winton, M., Wittenberg, A. T., Xiang, B., Zadeh, N., and Zhang, R. 2019 The GFDL global ocean and sea ice model OM4.0: Model description and simulation features, *Journal of Advances in Modeling Earth Systems*, **11**(10), 3167–3211.

Benjamin, M. R., Schmidt, H., and Newman, P. 2021 *An Overview of MOOSIvP and a Users Guide to the IvP Helm – Release 19.8*, Cambridge, MA: Department Mechanical Engineering Massachusetts Institute of Technology and Oxford, England: Department of Engineering Science University of Oxford.

Chaloner, K. and Verdinelli, I. 1995 Bayesian experimental design: A review, *Statistical Science*, **10**, 273–304.

Doerry, A. 2008 Ship dynamics for maritime ISAR imaging, SAND2008-1020, 929523.

Du, X., Zheng, Z., and Guan, S. 2018 Numerical calculation of hydrodynamic interactions of submarine flow on AUV. In: *2018 OCEANS – MTS/IEEE Kobe Techno-Oceans (OTO)*. OCEANS - MTS/IEEE Kobe Techno-Ocean (OTO), Kobe, Japan: IEEE, pp. 1–5.

Ellis, G. 2012 Four types of controllers, In: *Control System Design Guide*, Oxford, UK: Butterworth-Heinemann, pp. 97–119.

Fedor, R. 2009 Simulation of a launch and recovery of an UUV to an submarine, thesis. Royal Institute of Technology.

Fossen, T. I. 2011 *Handbook of Marine Craft Hydrodynamics and Motion Control*, Hoboken, New Jersey, U.S.: John Wiley & Sons, Ltd.

Groves, N. C., Huang, T. T., and Chang, M. S. 1989 *Geometric Characteristics of DARPA SUBOFF Models*, David Taylor Research Center.

Hammond, B. M. and Sapsis, T. P. 2023 Reduced order modeling of hydrodynamic interactions between a submarine and unmanned underwater vehicle using nonmyopic multi-fidelity active learning, *Ocean Engineering*, **288**(Part I), 1–18.

Healey, A. J. and Lienard, D. 1993 Multivariable sliding mode control for autonomous diving and steering of unmanned underwater vehicles, *IEEE Journal of Oceanic Engineering*, **18**, 14.

Jayarathne, B. N., Ranmuthugala, D., Chai, S., and Fei, J. 2014 Accuracy of potential flow methods to solve real-time ship-tug interaction effects within ship handling simulators, *TransNav, the International Journal on Marine Navigation and Safety of Sea Transportation*, **8**(4), 497–504.

Leong, Z. Q. 2014 Effects of hydrodynamic interaction on an AUV operating close to a moving submarine, PhD thesis, Australian Maritime College, University of Tasmania.

McCreight, K. K. 1998 *A Note on the Selection of Wave Spectra for Design Evaluation*, Naval Surface Warfare Center.

NATO. 2022 *Multi-National Submarine and Anti-Submarine Exercise Manual*, NATO.

Newman, J. N. 2017 *Marine Hydrodynamics*, 40th Anniversary, Cambridge, MA: MIT Press.

Osborn, T. R. and Lueck, R. G. 1985 Turbulence measurements with a submarine, *Journal of Physical Oceanography*, **15**(11), 1502–1520.

Perez, T., Donaire, A., and Valentinis, F. 2018 Parametric modelling of interacting hydrodynamic forces in underwater vehicles operating in close proximity, *IFAC-PapersOnLine*, **51**(29), 92–97.

Pickering, E., Guth, S., Karniadakis, G. E., and Sapsis, T. P. 2022 Discovering and forecasting extreme events via active learning in neural operators, *Nature Computational Science*, **12**(2), 823–833.

Prestero, T. 2001 *Verification of a Six-degree of Freedom Simulation Model for the REMUS Autonomous Underwater Vehicle*, Woods Hole, MA: Massachusetts Institute of Technology and Woods Hole Oceanographic Institution.

Rasmussen, C. E. and Williams, C. K. I. 2006 *Gaussian Processes for Machine Learning*. Adaptive computation and machine learning. Cambridge, MA: MIT Press, 248 p.

Sacks, J., Welch, W. J., and Mitchell, T. J. 1989 Design and analysis of computer experiments, *Statistical Science*, **4**, 409–423.

SNAME. 1950 Nomenclature for treating the motion of a submerged body through a fluid, Technical and Research Bulletin, 16.

Warner, D. C. 1991 Design, simulation, and experimental verification of a computer model and enhanced position estimator for the NPS AUV II, thesis, Naval Postgraduate School.